ACS APPLIED MATERIALS & INTERFACES

Research Article

Cite This: ACS Appl. Mater. Interfaces 2019, 11, 23207−23212

www.acsami.org

Gassing in Sn-Anode Sodium-Ion Batteries and Its Remedy by Metallurgically Prealloying Na

Wenjian Liu,[†,‡] Xinlong Chen,[†,‡] Can Zhang,[†,‡] Hui Xu,[†,‡] Xin Sun,[†,‡] Yuheng Zheng,[†,‡] Yue Yu,[†,‡] Sa Li,*[,†,‡] Yunhui Huang,[†,‡] and Ju Li*[,§]

[†]School of Materials Science and Engineering and [‡]Institute of New Energy for Vehicles, Tongji University, Shanghai 201804, China

[§]Department of Nuclear Science and Engineering and Department of Materials Science and Engineering, Massachusetts Institute of Technology, Cambridge, Massachusetts 02139, United States

Supporting Information

ABSTRACT: Despite the high theoretical energy densities of tin as the anode of sodium-ion batteries, its electrochemical performance has been plagued by the inadequate initial Coulombic efficiency (ICE) and poor cycle life. While it is generally believed that mechanical degradation, namely, pulverization and subsequent loss of electrical contact, is the underlying cause, here, we show that gassing is an essential problem in sodium-ion batteries with Sn anode. Since the gas generation appears at a certain voltage, reducing the voltage by metallurgically prealloying Sn with Na could be a solution, with an additional benefit of compensating for "live" Na loss in future cycles. When the metallurgically alloyed foil is used as the anode in $Na_3V_2(PO_4)_2F_3$ (NVPF)// alloy full cells, the ICE is significantly improved from 24.68 to 75%, and from the 2nd cycle to the 100th cycle, the average Coulombic efficiency can be maintained up to 99.44%. The full cell can run for 100 cycles, with acceptable capacity decay to 81.4 mAh/g(NVPF) from the initial 112.5 mAh/g(NVPF).

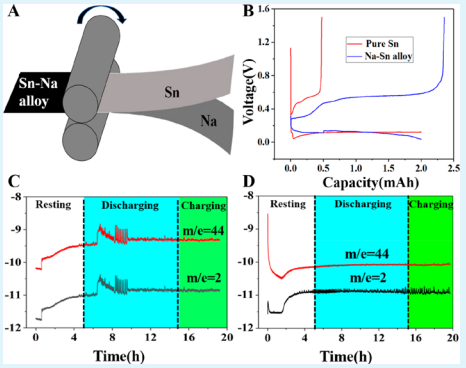

KEYWORDS: *solid-electrolyte interphase, gassing, presodiation, electrolyte decomposition, initial Coulombic efficiency*

1. INTRODUCTION

While Li-ion batteries (LIBs) are widely used in portable electronic devices during the last several decades,[1] they may be not suitable for larger scale energy storage for their scarce and uneven distribution and high price.[2,3] Sodium shows roughly similar properties as lithium, and more importantly, it is much more abundant, which makes sodium-ion battery (SIB) an appealing alternative.[4,5] Several promising Na-ion battery cathodes such as Na_xCoO_2, $Na_2Fe_2(SO_4)_3$, $Na_3V_2(PO_4)_3$, and $Na_xNi_{0.22}Co_{0.11}Mn_{0.66}O_2$ have been reported to exhibit decent properties.[6,7] Therefore, finding a competitive anode is imperative. Sn (on the same column as carbon) has attracted some attention for its high theoretical gravimetric specific capacity of 847 mAh/g, electrical conductivity, low reaction potential, earth abundance, and by virtue of high density (7.31 g cm^{-3}) a high volumetric energy density. Thus, it should be applicable to be the anode material in the Na-ion battery.[4,8] Previously, most efforts were focused on extending the cycling life by designing various nanostructures and composites.[9,10] However, refining the anode materials into nanoscale brings a larger surface area between the electrode and electrolyte, leading to various parasitic reactions and consumption of large amount of "live" Na inventory as well as the electrolyte during cycling, which would severely deteriorate the Coulombic efficiency especially in the first several cycles.[11]

On the other hand, metallic Sn foil could be an outstanding candidate as a self-supporting anode of SIBs, considering its good electrical conductivity, mechanical ductility for processing, weight, volume, and cost savings because of the elimination of current collectors and binders. It has been reported that metal or alloy foils could be utilized as the anode directly,[12,13] and that the Sn foil can be applied in SIBs.[14,15] For Sn foil, the generic problems of Sn nanoparticles still exist, which is the dramatic volume expansion/shrinkage of up to 420% during charging/discharging:[5,16] the repeated volume change would cause (a) breaking and reformation of the solid electrolyte interphase (SEI) film on the anode, converting the "live" or cyclable sodium in the electrolyte and electrodes to noncyclable sodium and killing the batteries eventually by exhausting sodium or the electrolyte in the system, and (b) mechanical failure, namely, pulverization and subsequent loss of electrical contact from the current collector. However, it is worth mentioning that the above two damage mechanisms are not necessarily the only explanations for the poor electrochemical performance. Especially, when considering the intrinsic chemical/electrochemical properties of Sn, which has an electron configuration of $4d^{10}$ $5s^2$ $5p^2$ and can function

Received: March 21, 2019
Accepted: May 29, 2019
Published: May 29, 2019

DOI: 10.1021/acsami.9b05005
ACS Appl. Mater. Interfaces 2019, 11, 23207−23212

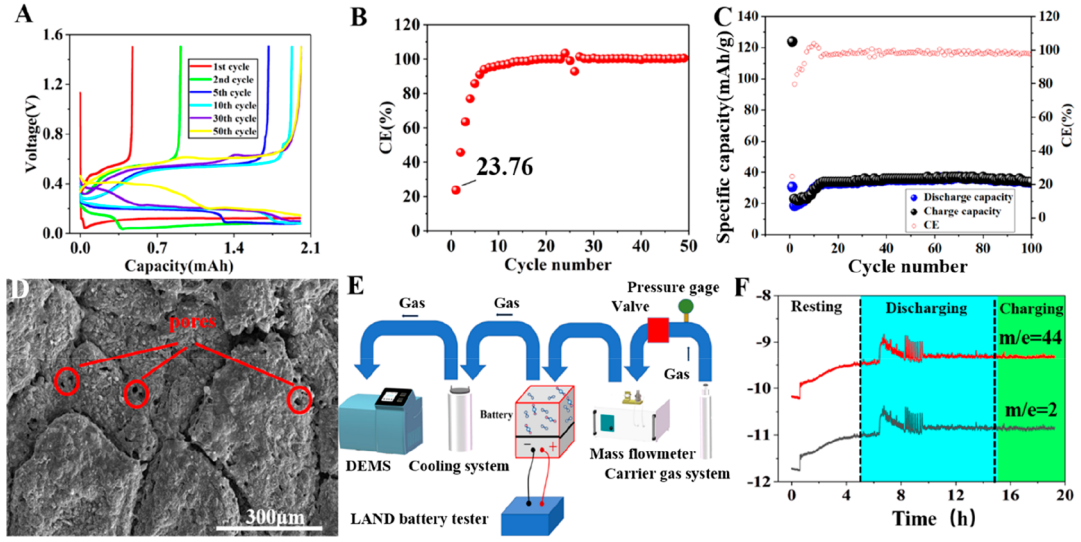

Figure 1. Characterization and electrochemical evaluation of the pure tin system. (A) Voltage profiles of the Sn//Na half cell. (B) Coulombic efficiency (CE) profile of the Sn//Na half cell. (C) Electrochemical performance data of the NVPF//Sn full cell. (D) SEM image of the cycled Sn surface. (E) Gas analysis setups. (F) Differential electrochemical mass spectrometry result of the NVPF//Sn full cell.

as the catalyst of many organic transformations, some other possible degradation mechanisms associated with electrolyte decomposition should be studied.

Herein, we first confirmed that the poor ICE (25%) of Sn foil anode is mostly attributed to the serious gas generation, revealed by *in operando* as well as post-mortem characterizations. Based on this revelation, we develop a strategy of metallurgically prealloying Na to reduce the open-circuit voltage (OCV) and suppress the gas release. Encouragingly, when the alloy foil is used as the anode in $Na_3V_2(PO_4)_2F_3$(NVPF)//Na-Sn full cells, the ICE is significantly improved from 25 to 75%, and from the 2nd cycle to the 100th cycle, the average Coulombic efficiency can be maintained up to 99.44%. After 100 cycles, the cathode-weight normalized capacity is reduced to a still-acceptable value of 81.4 mAh/g (NVPF) from 112.5 mAh/g (NVPF). After presodiation, the OCV of the Na−Sn alloy anode is generally lower than the gassing voltage in the first cycle, and the products of electrolyte decomposition tend to be solid and therefore facilitate a complete coverage of the SEI on the anode surface. The gassing behavior will continuously destroy the SEI and result in the rebuilding of SEI repeatedly, leading to a significant consumption of active sodium ions. Therefore, suppressing the gassing would improve ICE to some degree. However, it is worth mentioning that the improvement of ICE could also be attributed to presodiation itself because sodium has been stored in the anode material to compensate for the lost sodium ions. We confirmed that the electrochemical cycling stability of the alloy foil is actually much improved than that of either the bare sodium or the bare Sn foil. Furthermore, the alloy anode can retain such superior electrochemical properties even after a certain period of ambient air exposure.

2. RESULTS AND DISCUSSION

In our study, the tin foil serves as the free-standing anode directly instead of the tin-based nanostructure powder on some other current collector. Generally speaking, since the true surface area of Sn foil is largely reduced compared with that of the powders, the ICE of Sn foil is expected to be better than that of the Sn particles, which, however, is not the case from Figure 1A−C. The variation of the curves represents different alloying reactions in half-cells versus superabundant Na metal counter-electrode. There are three plateaus of different discharge curves at 0.40, 0.23, and 0.12 V versus Na^+/Na (Figure 1A), which represent $NaSn_2$, Na_9Sn_4, and $Na_{15}Sn_4$ alloying reactions, respectively. In the first cycle, the gassing is severe, and the bubbles would cover most part of the Sn foil, which leads to the decrease in the active Sn area reacting with the Na ions. However, the total fluence of the Na ions during the sodiation process is constant (~2 mAh every cycle), meaning that the average amount of Na ions that are alloyed by Sn per active area would be higher considering the lower accessible Sn surface in the first few cycles. Therefore, it tends to form a sodium-rich alloy, and the voltage plateau is low. In the following cycles, because of the suppresion of bubble formation as more and more SEIs are generated, and meanwhile, some gases would also start to detach from the Sn anode, exposing a larger active Sn surface area for sodiation and thus lowering the sodiation degree for each Sn atom, which renders a higher voltage plateau. As a result, the curves of different discharge cycles have the variation, and correspondingly, similar results occur to the charge curves. Meanwhile, there is a high hysteresis during charge/discharge cycling (Figure 1A) that originated from the gas release in the electrochemical reactions. It is generally accepted that when gases are produced in the cell, there would be a corresponding increase in the internal resistance[17] and thus resulting in potential variations for both charge and discharge profiles. Besides, with the prolonged cycling, the SEI thickness would increase as well, which could be an underlying reason for the big gap between charge and discharge curves.[18] From the Coulombic efficiency profiles of the Sn//Na half cell (Figure 1B) and NVPF//Sn full cell (Figure 1C and Figure S1D), although both cells show stabilized performance since the 10th cycle, the ICE is surprisingly as low as 24.68 and 23.76%, respectively, and the full cell CE gradually rises to 98.97% until the 7th cycle. From the 8th cycle, the average Coulombic efficiency reaches up to 98%, and can maintain 100 cycles at least. To figure out the underlying cause of the poor ICE, we disassembled the half cell after 100 cycles and characterized the

DOI: 10.1021/acsami.9b05005
ACS Appl. Mater. Interfaces 2019, 11, 23207−23212

Scheme 1. Proposed Gassing Mechanisms for (A) ethylene carbonate (EC), (B) dimethyl carbonate (DEC), and (C) fluoroethylene carbonate (FEC)

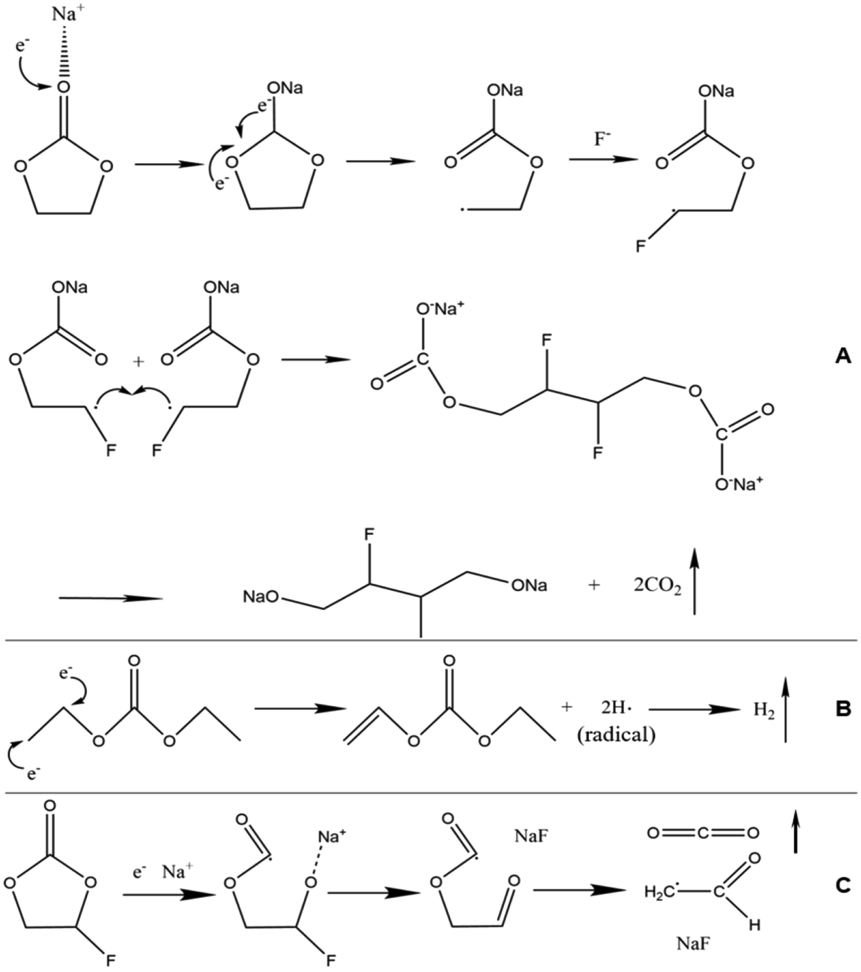

surface of the cycled Sn anode. It can be seen from the scanning electron microscopy (SEM) image (Figure 1D) that some pores distribute on the cycled Sn surface,[19] which seem to be left by gas vents. To affirm this, differential electrochemical mass spectrometry (DEMS) measurements were carried out to characterize the gases released. The gas analysis setups are illustrated in Figure 1E, and as can be seen in Figure 1F, after 5 h resting, gases start to evolve almost at the same time at the first 1 h discharging, which are identified to be CO_2 and H_2 according to the mass spectrometer charge-to-mass ratio analysis, and the proposed gas generation mechanisms are shown in Scheme 1A–C.[20−22] In the previous research on Li-ion batteries, gaseous components were detected in various anode materials as electrolyte decomposition by-products that were usually accompanied by solid species (that will eventually build up the SEI), such as Li metal,[23] graphite,[23] silicon,[23] and LTO.[24] The presence of gaseous products (instead of solid products) and detaching gas bubbles, however, would inevitably erode the emergent SEI film on the anode surface, leading to spallation and reformation of SEI passivation in the following cycles. Moreover, it might also form a layer of gas on the Sn surface that will separate the Sn electrode with electrolyte and cut off the sodium transport path largely.

From previous studies of ethylene carbonate (EC), dimethyl carbonate (DEC), and fluoroethylene carbonate (FEC)-containing electrolytes, it was estimated that in the LIB system, the EC decomposition voltage varies within the range of 0.35 to 0.65V[21] versus Li^+/Li, and the DEC decomposition voltage is estimated at ∼1.0V[21] while the FEC is at ∼1.37 V.[22] It is well accepted that the solvent in the electrolyte would decompose when the redox potential of the electrodes used in a battery lies outside the electrochemical stability window of the electrolyte. According to previous reports, both the salt species and salt concentration would influence the decomposition voltages of the solvent.[25] Interestingly, it seems that the salt concentration largely influences the reductive decomposition voltage of the solvent, while the salt species play a significant role in oxidative decomposition voltage of the solvent. Therefore, at the anode side, we assume that salt species barely affect the decomposition voltage for the same solvent of the same salt concentration. Thus, we assume that the decomposition voltage are similar for the same solvent in either lithium salts or sodium salts of the same concentration.[15] Generally speaking, the reductive decomposition of electrolyte molecules can lead to gaseous products, solid products, or liquid-soluble products, with varying ratios that should depend on the voltage. Based on our experimental phenomenon, we speculate that the intermediate voltages below the electrochemical stability window could be divided into several stages: (1) harmful side reactions occur at 1.4−0.5 V that produce gases as well as gas film which suppress adherent SEI formation; (2) at even lower potential, for example, 0.5−0.4

DOI: 10.1021/acsami.9b05005
ACS Appl. Mater. Interfaces 2019, 11, 23207−23212

V, the gassing stops and beneficial side reactions take place to form a stable SEI layer on the Sn anode; and (3) when the potential reaches the discharge platform voltage, main alloying reactions initiate, and meanwhile, some beneficial SEI formation reaction might also continue. Therefore, once Sn is presodiated, the OCV is largely lowered down to ~0.4 V, and the stage of harmful side reactions is then bypassed. However, the situation would be much more complicated for the pristine Sn anode, once gases are created in the cell. Specifically, with the release of gases, there would be a large increase in the internal resistance and subsequently a great voltage drop, usually down to discharge platform potentials. Note that there would be extremely inhomogeneous current distribution that is related to gas adsorption/desorption on the anode surface. We hypothesize that, electrode voltages on the lower end closer to the Li^+/Li preferentially lead to solid products that build up the SEI passivation, while intermediate voltages just below the electrochemical stability window (e.g., ~1.0 and ~1.37 V above) lead preferentially to gassing, similar to the well-known voltage-dependent immune → active and active → passive behavior in the corrosion of metals, where the active → passive transition is attributed to the formation of a compact all-covering solid passivation layer, while the immune → active transition is characterized by a finite driving force and nonstoppage of side reactions (in our case, self-perpetuating and continuous gas generation that disrupts the SEI buildup). Therefore, lowering the open-circuit voltage (OCV) of the Sn anode is expected to avoid the gas generation to facilitate the formation of the compact SEI film. The lower OCV would provide a higher driving force for forming an SEI, which is self-limiting instead of self-perpetuating.

Thus, we develop a process (Figure 2A and Figure S2) of metallurgically prealloying sodium in this study, and successfully lower the OCV to ~0.2 V versus Na^+/Na, to suppress gassing upon the very first contact with the electrolyte. As illustrated in Figure 2, the tin metal foil (digital picture shown in Figure 2C) and sodium metal foil (digital picture shown in Figure 2D) were roll-to-roll pressed to in situ produce Na−Sn alloy (dark gray in the digital picture shown in Figure 2E) with larger surface roughness. To clearly illustrate the presodiation process of Sn foil, we record the production process as shown in Figure S2 and Video S1 in the Supporting Information. To confirm the success of metallurgically alloying, the X-ray diffraction (XRD) pattern of the post-treatment sample is shown in Figure 2B, which reveals the existence of $Na_{29.58}Sn_8$ and Na_9Sn_4. From the SEM image of the cross section of the post-treatment sample in Figure 2F, it is apparently divided into two parts, the upper part is about 70.6 μm and the lower part is 76.5 μm. According to the line scanning of energy spectrum along the arrow in Figure 2G, tin and sodium are both found in the lower part, which can prove that the Na−Sn alloy is formed, and the upper half part is the pristine Sn metal.

DEMS is adopted to verify the suppression of gassing, and as shown in Figure 3A, no gas is detected during cycling, meaning

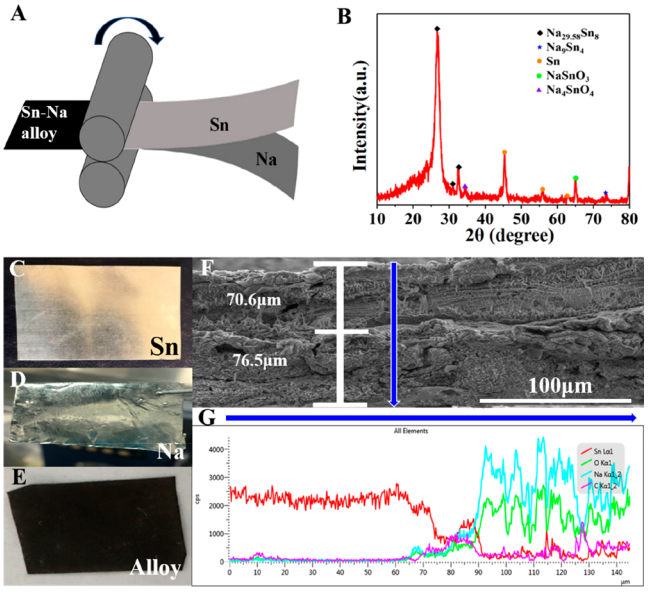

Figure 2. Preparation and characterization of the Na−Sn alloy. (A) Diagrammatic drawing of the metallurgical prealloying process. (B) X-ray diffraction (XRD) pattern of the post-treatment sample. (C) Digital picture of pure tin foil and (D) Digital picture of the sodium foil. (E) Digital picture of the Na−Sn alloy. (F) SEM image of the cross section of the post-treatment sample. (G) Line scanning of the energy spectrum of the post-treatment sample.

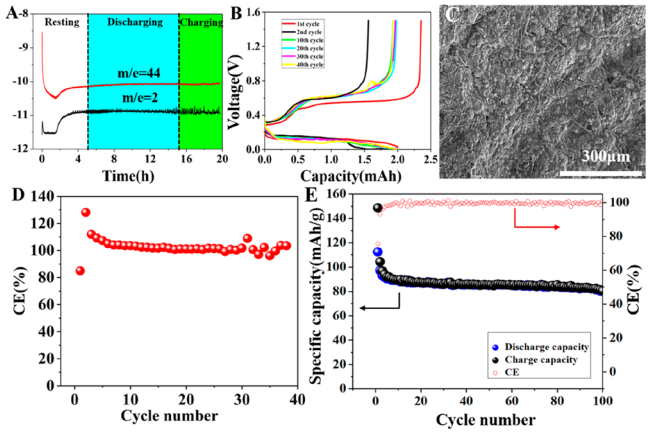

Figure 3. Characterization and electrochemical evaluation of the alloy system. (A) DEMS result of the NVPF//Na−Sn alloy full cell. (B) Voltage profiles of Na−Sn alloy//Na half cell. (C) SEM image of the cycled Na−Sn alloy. (D) CE profile of the Na−Sn//Na half cell. (E) Cycle performance of the NVPF//Na−Sn full cell.

that the lower OCV facilitates solid by-products (SEI) instead of gaseous species formation, and thus, gas generation has been effectively mitigated. Figure 3B shows the voltage profiles of the Na−Sn//Na half cell, and the discharge voltage plateaus basically stabilize at ~0.12 V, which is obviously much steadier than that in the Sn//Na half cell (Figure 1A). In addition, the starting voltage of the charging curve seems too high because during the battery test process, there is a period of resting for 10 min between charging and discharging. The detailed potential changes are demonstrated in Figure S4, and it can be observed that the potential gradually increases to ~0.2 V when conducting resting after discharging, and on the other hand, the potential would gradually get down to ~0.55 V when conducting resting after charging. The cycle performances of the Sn//Na half cell and NVPF//Na−Sn full cell are shown in Figure 3D,E and Figure S1E. The full cell ICE can reach 75%, which is much higher than the counterpart with the pristine tin anode (shown in Figure 1C) and even better than most of the nanostructured Sn and Sn-based composites (Table S1). More encouragingly, the Coulombic efficiency (CE) reaches 93.09%

DOI: 10.1021/acsami.9b05005
ACS Appl. Mater. Interfaces 2019, 11, 23207−23212

at the 2nd cycle and maintains an average value of 99.4% in the following 100 cycles. The specific capacity still remains 81.4 mAh/g(NVPF) after 100 cycles, corresponding to the 72.36% retention, which could be industrially acceptable for certain applications. We also compare the rate performance of NVPF//Sn full cell with NVPF//Na−Sn full cell in Figure S3A, where an obvious superiority could be observed after presodiation. Also, the CV profiles (Figure S3B) show that the Na−Sn alloy profiles have two peaks at ∼0.48 and ∼0.68 V, which means that two alloying reactions occur during charging. The pure Sn profile has only one peak at ∼0.66 V, and single alloying reaction occurs. Besides, the peaks of Na−Sn alloy profiles are much higher than that of the pure Sn profile, which indicates that after presodiation, the cell has a much larger capacity. Also, from the SEM image of the cycled Na−Sn alloy (Figure 3C), no obvious holes or cracks are left by gas vents. It is worth mentioning that compared with the previously reported presodiation approaches, including (1) electrochemical pre-sodiation, which requires one to disassemble the half-cell after the electrochemical sodium insertion and then pairing it with the cathode, (2) introducing sodium compounds such as NaN_3[26] and Na_3P,[27] both of which are expensive to obtain, and (3) utilizing sodium powder that is produced through an ultrasound-assisted synthesis,[28] which is complicated and demands a highly inert environment, our approach is cheap and scalable and more applicable to industry.

The air stability of the electrode materials is extremely important for the battery industry, especially during handling and battery assembly. High sensitivity to ambient environment would often greatly increase the cost of industrial manufacturing. Therefore, we further examine the air stability of the alloy by opening the sealing bag and exposing it to ambient air for 1 and 2 h. After various periods of exposure, no difference could be visually observed (Figure S1A−C). As for the electrochemical performance, both the Na−Sn//Na half cell and NVPF//Na−Sn full cells were examined. It can be seen from Figure 4B that the discharge voltage plateaus are ∼0.14 V and

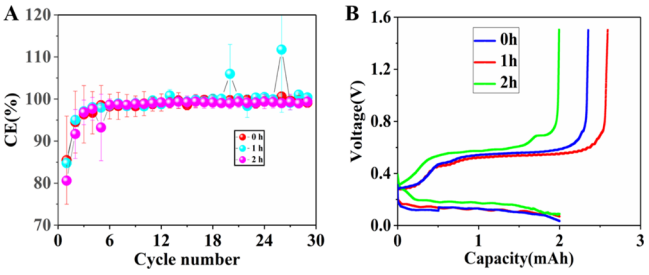

Figure 4. Electrochemical evaluation of the anodes placed for different hours. (A) CE of the Na−Sn//Na half cells respectively with error bars. (B) First-cycle voltage profiles of the Na−Sn//Na half cell using the anodes placed in the air for 0, 1, and 2 h.

are almost the same, which proves that the discharge voltage is stable. As shown in Figure 4A, after exposure in air for up to two hours, the alloy foil can still perform efficiently in NIBs. All of the first-cycle Coulombic efficiencies are above 75%, and the Coulombic efficiency can exceed 99% from the 2nd cycle, which shows that the stability of the alloy is quite reliable when compared with the pure sodium metal foil. To further illustrate the superior performance of this alloy anode, a NVPF//Na−Sn full cell with a Na−Sn foil that has been exposed in the air for 2 h was made, and the result is shown in Figure S1F. The average CE of the 50 cycles is more than 97.7% except for the first cycle. After 50 cycles, the specific capacity can still remain above 70 mAh/g(NVPF), which again demonstrates the acceptable air stability of the alloy anode.

3. CONCLUSIONS

As an SIB anode candidate, metallic tin has traditionally suffered from low ICE and poor cycle life. While most research studies attributed the inadequacy to mechanical failure, we revealed severe gassing issue of the pure Sn anode, due to high open-circuit voltage that facilitates gaseous electrolyte-decomposition-products. Based on the in situ DEMS analysis, the gas generation mechanisms were proposed. The detrimental effect of gases is attributed to the interfacial forces exerted by departing gas bubbles on the emergent SEI, which leads to SEI spallation as well as separation of the electrode from the electrolyte. Since the gassing reactions are voltage-controlled, a lower absolute electrode potential might suppress gassing and promote stable SEI formation when we examine the parallels to the well-known voltage-dependent immune → active and active → passive behavior in the corrosion of metals. Thus, we have developed a facile roll-to-roll metallurgical presodiation method to produce Sn−Na alloy foil and surprisingly found that the gassing behavior was significantly mitigated. Compared with the pristine tin anode, after metallurgically alloying Na, the ICE of the $Na_3V_2(PO_4)_2F_3$(NVPF)//Sn−Na full cell is boosted to 75 from 24.68%. The reversible capacity based on the NVPF cathode material maintains at 72% after 100 cycles. It is also worth mentioning that the Sn−Na alloy anode shows decent air stability. Our study provides a new insight into the degradation mechanism of metallic foil-based anodes in SIBs, and the remediation strategy we developed here might also be applicable to other metallic anode candidates.

■ ASSOCIATED CONTENT

Supporting Information

The Supporting Information is available free of charge on the ACS Publications website at DOI: 10.1021/acsami.9b05005.

Detailed methods and additional supporting data (PDF)

Whole process of presodiation (MP4)

■ AUTHOR INFORMATION

Corresponding Authors

*E-mail: lisa@tongji.edu.cn (S.L.).

*E-mail: liju@mit.edu (J.L.).

ORCID

Ju Li: 0000-0002-7841-8058

Notes

The authors declare no competing financial interest.

■ ACKNOWLEDGMENTS

The authors are grateful for the support from Tongji University and the National Natural Science Foundation of China (NSFC, nos. 51602222 and 51632001). W.L., X.C., and C.Z. acknowledge the support by the National College Students Innovation and Entrepreneurship Training Program (no.0500107107). S.L. acknowledges the support by the Fundamental Research Funds for the Central Universities (no. 0500219233). J.L. acknowledges support by NSF ECCS-

1610806. The authors are also grateful for the support from Shanghai Linglu Instrument Equipment Co., Ltd.

REFERENCES

(1) Hwang, J. Y.; Myung, S. T.; Sun, Y. K. Sodium-Ion Batteries: Present and Future. *Chem. Soc. Rev.* **2017**, *46*, 3529−3614.
(2) Palomares, V.; Serras, P.; Villaluenga, I.; Hueso, K. B.; Carretero-González, J.; Rojo, T. Na-Ion Batteries, Recent Advances and Present Challenges to Become Low Cost energy storage Systems. *Energy Environ. Sci.* **2012**, *5*, 5884−5901.
(3) Pan, H.; Hu, Y.-S.; Chen, L. Room-Temperature Stationary Sodium-Ion Batteries for Large-Scale Electric Energy Storage. *Energy Environ. Sci.* **2013**, *6*, 2338.
(4) Cui, J.; Yao, S.; Kim, J.-K. Recent Progress in Rational Design of Anode Materials for High-Performance Na-Ion Batteries. *Energy Storage Mater.* **2017**, *7*, 64−114.
(5) Yabuuchi, N.; Kubota, K.; Dahbi, M.; Komaba, S. Research Development on Sodium-Ion Batteries. *Chem. Rev.* **2014**, *114*, 11636−11682.
(6) You, Y.; Manthiram, A. Progress in High-Voltage Cathode Materials for Rechargeable Sodium-Ion Batteries. *Adv. Energy Mater.* **2018**, *8*, 1701785.
(7) Berthelot, R.; Carlier, D.; Delmas, C. Electrochemical Investigation of the P2-Na_xCoO_2 Phase Diagram. *Nat. Mater.* **2011**, *10*, 74−80.
(8) Datta, M. K.; Epur, R.; Saha, P.; Kadakia, K.; Park, S. K.; Kumta, P. N. Tin and Graphite Based Nanocomposites: Potential Anode for Sodium Ion Batteries. *J. Power Sources* **2013**, *225*, 316−322.
(9) Luo, W.; Shen, F.; Bommier, C.; Zhu, H.; Ji, X.; Hu, L. Na-Ion Battery Anodes: Materials and Electrochemistry. *Acc. Chem. Res.* **2016**, *49*, 231−40.
(10) Dai, K.; Zhao, H.; Wang, Z.; Song, X.; Battaglia, V.; Liu, G. Toward High Specific Capacity and High Cycling Stability of Pure Tin Nanoparticles with Conductive Polymer Binder for Sodium Ion Batteries. *J. Power Sources* **2014**, *263*, 276−279.
(11) Baggetto, L.; Ganesh, P.; Meisner, R. P.; Unocic, R. R.; Jumas, J.-C.; Bridges, C. A.; Veith, G. M. Characterization of Sodium Ion Electrochemical Reaction with Tin Anodes: Experiment and Theory. *J. Power Sources* **2013**, *234*, 48−59.
(12) Wang, M.; Jiang, C.; Zhang, S.; Song, X.; Tang, Y.; Cheng, H. M. Reversible Calcium Alloying Enables a Practical Room-Temperature Rechargeable Calcium-Ion Battery with a High Discharge Voltage. *Nat. Chem.* **2018**, *10*, 667−672.
(13) Jiang, M.; Yu, Y.; Fan, H.; Xu, H.; Zheng, Y.; Huang, Y.; Li, S.; Li, J. Full-Cell Cycling of a Self-Supporting Aluminum Foil Anode with a Phosphate Conversion Coating. *ACS Appl. Mater. Interfaces* **2019**, *11*, 15656−15661.
(14) Jiang, C.; Fang, Y.; Zhang, W.; Song, X.; Lang, J.; Shi, L.; Tang, Y. A Multi-Ion Strategy towards Rechargeable Sodium-Ion Full Batteries with High Working Voltage and Rate Capability. *Angew. Chem., Int. Ed.* **2018**, *57*, 16370−16374.
(15) Sheng, M.; Zhang, F.; Ji, B.; Tong, X.; Tang, Y. A Novel Tin-Graphite Dual-Ion Battery Based on Sodium-Ion Electrolyte with High Energy Density. *Adv. Energy Mater.* **2017**, *7*, 1601963.
(16) Wang, J. W.; Liu, X. H.; Mao, S. X.; Huang, J. Y. Microstructural Evolution of Tin Nanoparticles During in Situ Sodium Insertion and Extraction. *Nano lett.* **2012**, *12*, 5897−5902.
(17) Han, M.; Zhu, C.; Zhao, Q.; Chen, C.; Tao, Z.; Xie, W.; Cheng, F.; Chen, J. In Situ Atomic Force Microscopic Studies of Single Tin Nanoparticle: Sodiation and Desodiation in Liquid Electrolyte. *ACS Appl. Mater. Interfaces* **2017**, *9*, 28620−28626.
(18) Li, L.; Jacobs, R.; Gao, P.; Gan, L.; Wang, F.; Morgan, D.; Jin, S. Origins of Large Voltage Hysteresis in High-Energy-Density Metal Fluoride Lithium-Ion Battery Conversion Electrodes. *J. Am. Chem. Soc.* **2016**, *138*, 2838−2848.
(19) Mateos, A. J.; Huang, W.; Zhang, Y.-W.; Greer, J. R. Discrete-Continuum Duality of Architected Materials: Failure, Flaws, and Fracture. *Adv. Funct. Mater.* **2018**, *29*, 1806772.
(20) Bridel, J.-S.; Grugeon, S.; Laruelle, S.; Hassoun, J.; Reale, P.; Scrosati, B.; Tarascon, J.-M. Decomposition of Ethylene Carbonate on Electrodeposited Metal Thin Film Anode. *J. Power Sources* **2010**, *195*, 2036−2043.
(21) Horowitz, Y.; Han, H. L.; Ross, P. N.; Somorjai, G. A. In Situ Potentiodynamic Analysis of the Electrolyte/Silicon Electrodes Interface Reactions–A Sum Frequency Generation Vibrational Spectroscopy Study. *J. Am. Chem. Soc.* **2016**, *138*, 726−729.
(22) Purushotham, U.; Takenaka, N.; Nagaoka, M. Additive Effect of Fluoroethylene and Difluoroethylene Carbonates for the Solid Electrolyte Interphase Film Formation in Sodium-ion Batteries: A Quantum Chemical Study. *RSC Adv.* **2016**, *6*, 65232−65242.
(23) Borodin, O.; Bedrov, D. Interfacial Structure and Dynamics of the Lithium Alkyl Dicarbonate SEI Components in Contact with the Lithium Battery Electrolyte. *J. Phys. Chem. C* **2014**, *118*, 18362−18371.
(24) Li, X.; Xu, J.; Huang, P.; Yang, W.; Wang, Z.; Wang, M.; Huang, Y.; Zhou, Y.; Qu, M.; Yu, Z.; Lin, Y. In-situ Carbon Coating to Enhance the Rate Capability of the $Li_4Ti_5O_{12}$ Anode Material and Suppress the Electrolyte Reduction Decomposition on the Electrode. *Electrochim. Acta* **2016**, *190*, 69−75.
(25) Geng, C.; Buchholz, D.; Kim, G.-T.; Carvalho, D. V.; Zhang, H.; Chagas, L. G.; Passerini, S. Influence of Salt Concentration on the Properties of Sodium-Based Electrolytes. *Small Methods* **2019**, *3*, 1800208.
(26) Martinez De Ilarduya, J.; Otaegui, L.; López del Amo, J. M.; Armand, M.; Singh, G. NaN_3 Addition, A Strategy to Overcome the Problem of Sodium Deficiency in P_2-$Na_{0.67}[Fe_{0.5}Mn_{0.5}]O_2$ Cathode for Sodium-ion Battery. *J. Power Sources* **2017**, *337*, 197−203.
(27) Zhang, B.; Dugas, R.; Rousse, G.; Rozier, P.; Abakumov, A. M.; Tarascon, J. M. Insertion Compounds and Composites Made by Ball Milling for Advanced Sodium-ion Batteries. *Nat. Commun.* **2016**, *7*, 10308.
(28) Tang, J.; Kye, D. K.; Pol, V. G. Ultrasound-assisted Synthesis of Sodium Powder as Electrode Additive to Improve Cycling Performance of Sodium-ion Batteries. *J. Power Sources* **2018**, *396*, 476−482.

DOI: 10.1021/acsami.9b05005
ACS Appl. Mater. Interfaces 2019, 11, 23207−23212

Supporting Information

Gassing in Sn-anode Sodium-ion Batteries and its Remedy by Metallurgically Pre-alloying Na

Wenjian Liu[1,2], Xinlong Chen[1,2], Can Zhang[1,2], Hui Xu[1,2], Xin Sun[1,2], Yuheng Zheng[1,2], Yue Yu[1,2], Sa Li[1,2], Yunhui Huang[1,2] and Ju Li[3*]*

[1] School of Materials Science and Engineering, Tongji University, Shanghai 201804, China

[2] Institute of New Energy for Vehicles, Tongji University, Shanghai 201804, China

[3] Department of Nuclear Science and Engineering and Department of Materials Science and Engineering, Massachusetts Institute of Technology, Cambridge, MA 02139, USA

[*]Corresponding authors' email:

lisa@tongji.edu.cn

liju@mit.edu

Methods

For metallurgically pre-alloying sodium, Na foil (150~200 μm) was stacked over Sn foil (100μm, 99.99%, Jinan Dingsheng Metal Materials Co., Ltd.) and the two foils were rolled together into Na-Sn alloy by a roller (MSK-2150, Shenzhen Kejing Star Technology, LTD.). The as-prepared alloy was punched into disks with 8 mm diameter. The whole procedure was carried out in an Argon-filled glove box. Then the Na-Sn alloys were exposed in ambient air for 0-2h and used as electrodes in NVPFs//Na-Sn full cells and Na-Sn//Na half cells. For a comparison, pristine Sn foil was punched into disks with 8 mm diameter and paired against commercial NVPFs cathode with a diameter of 8 mm in NVPFs//Sn full cells and sodium in Sn//Na half cells, respectively. The glass fiber separator (Whatman 1822-090) was used as separator in both full cell and half cells, and the electrolyte was 1 mol L^{-1} $NaClO_4$ dissolved in DEC/EC (v/v=1:1) with 5% FEC additive. Galvanostatic charge/discharge measurements were conducted in CR2032 coin cells by a Land battery testing system (CT2001A). The full cell was charged to 4.2 V and discharged to 2.0 V at a current density of 0.1 mA. The half cell was discharged to a fixed capacity of 2 mAh and charged to 1.5 V at a current density of 1 mA.

The XRD patterns of Sn-Na alloy was collected on a Bruker AXS GMBH GERM D8 Diffractometer with CuKα radiation (λ = 1.54184 Å) at a scan rate of 3° min^{-1}. The morphologies of the materials were obtained by **a FEI Quanta 200 scanning electron microscopy (SEM)**, and EDS (Energy Dispersive Spectrometer) line scanning spectrum of cross section was obtained simultaneously. The gas from the cell was analyzed by **Gas**

chromatography-mass spectrometry (GCMS, Finniga DSQ).

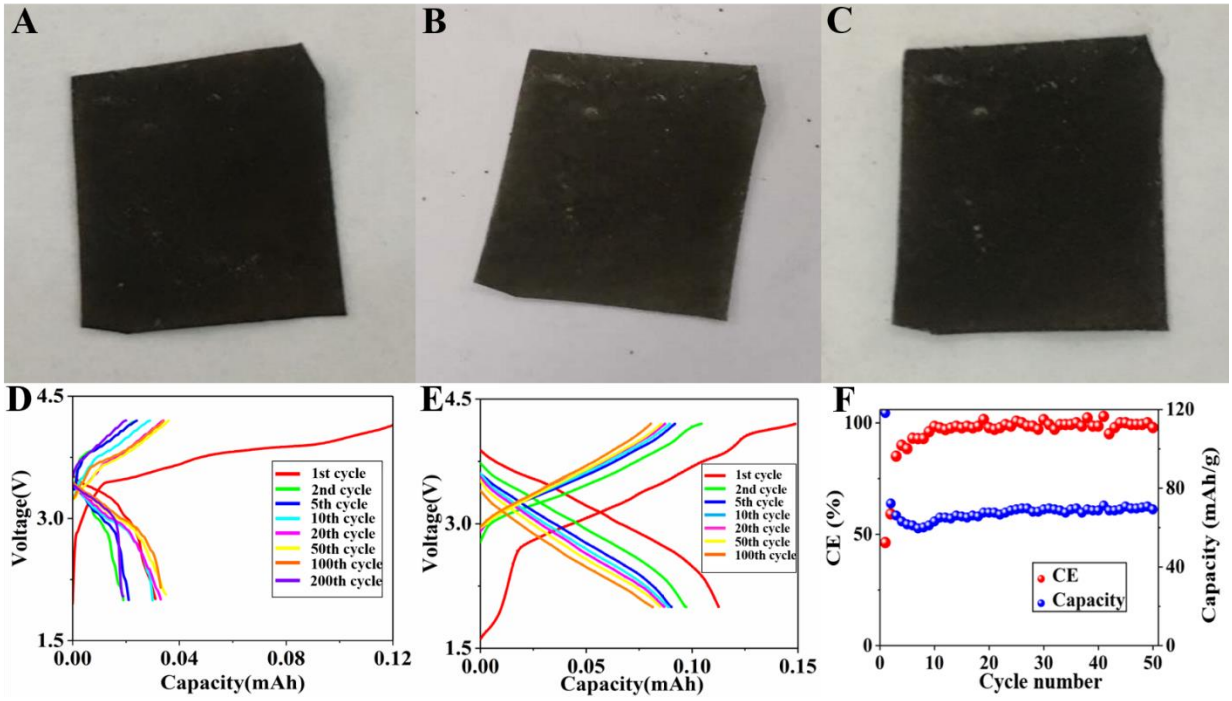

Figure S1 (A) The digital picture of the alloy placed in the air for 0h. (B) The digital picture of the alloy placed in the air for 1. (C) the digital picture of the alloy placed in the air for 2h. (D) the voltage profiles of the NVPFs//Sn full cell. (E) the voltage profiles of the NVPFs//Na-Sn full cell. (F) the cycling performance of the NVPFs//Na Sn full cell using the anodes exposed in the air for 2h.

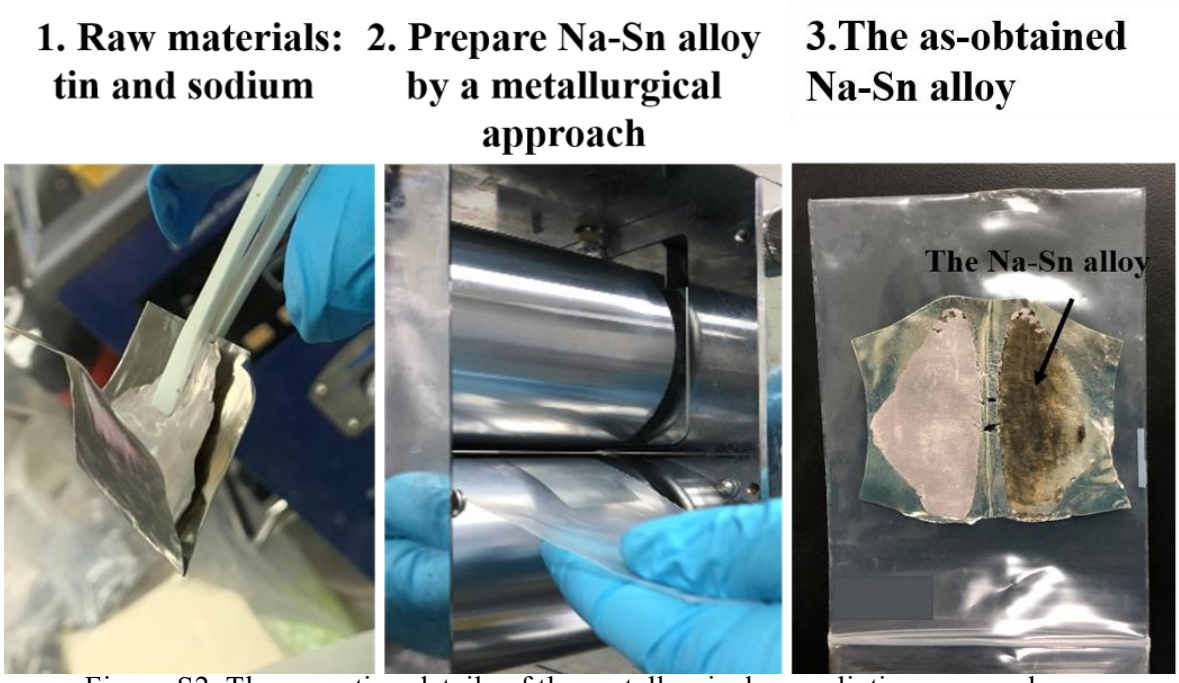

Figure S2. The operation details of the metallurgical presodiation approach.

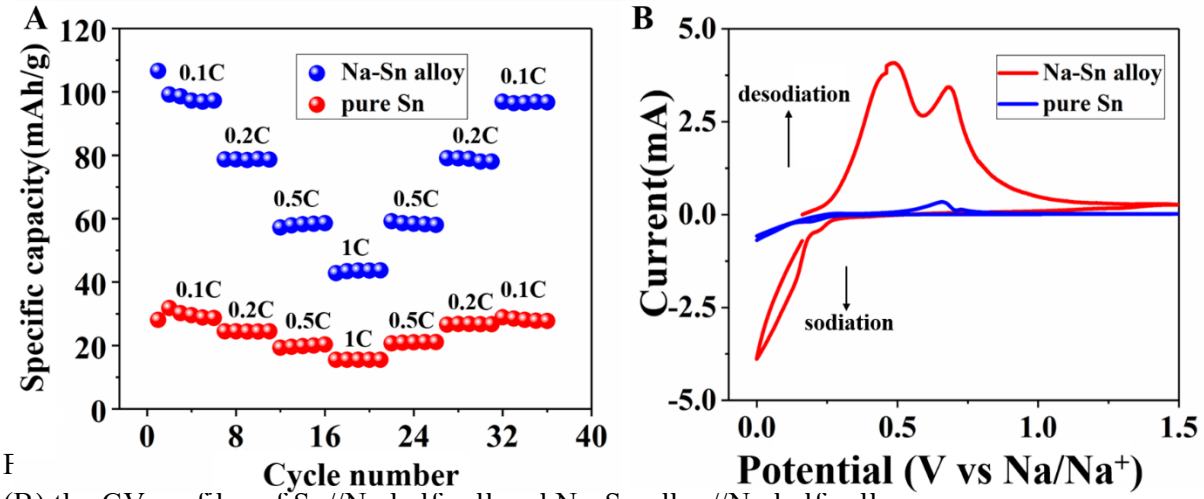

(B) the CV profiles of Sn//Na half cell and Na-Sn alloy//Na half cell.

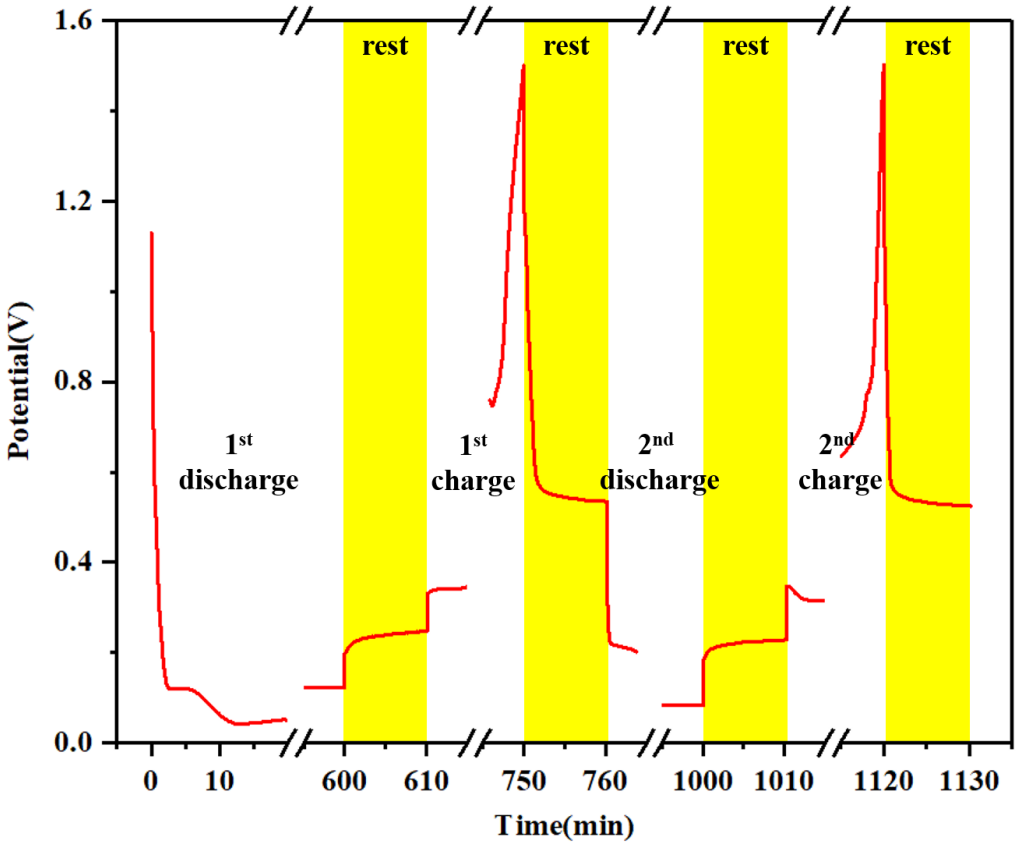

Figure S4. The Time-Potential profile of Sn//Na half cell.

Supplemental Video of presodiation process:

Video S1. The whole process of pesodiation.

Table S1. The performance of the Na-ion cell with the nano-structured Sn and Sn-based composites anode.

Anode material	Cycle index	ICE [%]	stable CE [%]	Initial capacity [mAh/g]	Ultimate capacity [mAh/g]	Capacity fading [%]	Current density
PSn[1]	500	63	99	674	519	33	0.5C
Sn/SnO_2/PC[2]	100	26	/	1148.1	265.4	76.90	50mA/g
TiO_2-Sn@CNFs[3]	400	58	>99.5	489.9	413	15.70	100mA/g
SnNP[4]	50	70.40	94	480	98.1	81	50mA/g
mSn/SnO_2[4]	50	46.80	96	750	372.3	50.36	50mA/g
Sn@NCNFs[5]	200	56	99	660	600	10	0.1C

REFERENCES

1. Kim, C.; Lee, K.-Y.; Kim, I.; Park, J.; Cho, G.; Kim, K.-W.; Ahn, J.-H.; Ahn, H.-J., Long-term cycling stability of porous Sn anode for sodium-ion batteries. Journal of Power Sources 2016, 317, 153-158.

2. Li, X.; Li, X.; Fan, L.; Yu, Z.; Yan, B.; Xiong, D.; Song, X.; Li, S.; Adair, K. R.; Li, D.; Sun, X., Rational design of Sn/SnO_2/porous carbon nanocomposites as anode materials for sodium-ion batteries. Applied Surface Science 2017, 412, 170-176.

3. Mao, M.; Yan, F.; Cui, C.; Ma, J.; Zhang, M.; Wang, T.; Wang, C., Pipe-Wire TiO2–Sn@Carbon Nanofibers Paper Anodes for Lithium and Sodium Ion Batteries. Nano letters 2017, 17 (6), 3830-3836.

4. Tang, D.; Huang, Q.; Yi, R.; Dai, F.; Gordin, M. L.; Hu, S.; Chen, S.; Yu, Z.; Sohn, H.; Song, J.; Wang, D., Room-Temperature Synthesis of Mesoporous Sn/SnO2 Composite as Anode for Sodium-Ion Batteries. European Journal of Inorganic Chemistry 2016, 2016 (13-14), 1950-1954.

5. Sha, M.; Zhang, H.; Nie, Y.; Nie, K.; Lv, X.; Sun, N.; Xie, X.; Ma, Y.; Sun, X., Sn nanoparticles@nitrogen-doped carbon nanofiber composites as high-performance anodes for sodium-ion batteries. Journal of Materials Chemistry A 2017, 5 (13), 6277-6283.